Dual-Pathway Polyolefin Upcycling over an Unexpectedly Bifunctional Low-Loading Ru/TiO_2-Anatase Catalyst

Linxiao Chen, Julia D. Moreira, Laura C. Meyer, Oliver Y. Gutiérrez, and János Szanyi*

Institute for Integrated Catalysis, Pacific Northwest National Laboratory, Richland, WA 99352, USA

*Corresponding author: janos.szanyi@pnnl.gov

Abstract

The large-scale production of non-degradable plastic waste calls for effective catalytic upcycling processes. In this work, we discovered that an anatase TiO_2 synthesized by a sol-gel method (TiO_2-A-SG) exhibits drastically better activity and selectivity as the support for low-loading Ru than other oxides in polypropylene (PP) upcycling under H_2. Detailed analysis and control experiments with Ni and Pt revealed that this is because Ru/TiO_2-A-SG also catalyzes hydrocracking besides hydrogenolysis. In addition to favoring high-valued liquid products, this increases branched alkane fraction from low-density polyethylene (LDPE), and allows efficient PP upcycling without noble metals. The unexpected Brønsted acidity of TiO_2-A-SG is linked to the carboxylate layers TiO_2 surfaces adsorb from air. Kinetic studies revealed that under testing conditions, the two pathways compete for dehydrogenated intermediates on metal surfaces, with low hydrogen pressure (P_{H2}) and high branching level of the substrate favoring hydrocracking. Hydrogenolysis is the main pathway at P_{H2} = 30 bar for all tested substrates less branched than PP, in which the cleavage of $^{2}C–^{2}C$ bonds is strongly favored over that of $^{3}C–^{x}C$ bonds. This work reveals and compares the two co-occurring polyolefin upcycling pathways on a metal-acid bifunctional catalyst, offers insights to the complex reaction network, and how it is affected by catalysts and conditions. In addition, it uncovers a new type of Brønsted acid sites on TiO_2 with deep implications in the broader scope of acid catalysis.

Keywords: plastic upcycling; hydrogenolysis; hydrocracking; polyolefins; titanium oxide

Introduction

The soaring, large-scale production of single-use plastics creates huge amount of non-degradable waste that severely threats the environment.[1, 2] The inefficacy of existing approaches for plastic waste processing, such as recycling and incineration,[3] leads to the demands for chemical routes that "upcycle" plastics into valuable chemicals. Besides environmental benefits, upcycling plastics also compensates for the oil consumption by their production[4] through circular economy. Polyolefins, including polypropylene (PP) and polyethylene (PE), are the most common types of plastics, making up > 50% of the annual production,[3] and also the most difficult to convert because they are entirely made of inert C−C single bonds. As a result, the upcycling of polyolefins requires either high temperature in pyrolysis,[5-7] which causes high energy consumption and low selectivity, or effective catalytic processes.

Two of the most promising routes for catalytic polyolefin upcycling are hydrogenolysis and hydrocracking. They require no additional feedstocks as metathesis or alkylation,[8, 9] and are less susceptible to deactivation than pyrolysis or Haag-Dessau cracking on monofunctional acidic catalysts.[6, 10, 11] Besides, these two reactions have been crucial parts of the oil refining industry and thus extensively studied with small alkane substrates, with established operation infrastructure and fundamental understanding partially applicable to polyolefin substrates. Both hydrogenolysis and hydrocracking refer to C−C bond cleavage under H_2 on supported metal catalysts, but the former cleaves C−C bonds on the metal, while the latter cleaves C−C bonds (and isomerizes substrates) on Brønsted acid sites after dehydrogenation on the metal, thus requiring metal-acid bifunctional catalysts. Despite initial success, the catalyst development for both routes is at a very preliminary stage. Meanwhile, polyolefins substrates often behave very differently from small alkanes,[12-14] and fundamental understanding specific to them is lacking. For hydrogenolysis, most studies used

catalysts with high noble metal (Ru or Pt) content,[12, 13, 15-25] and the selectivity needs to be steered away from low-valued gas alkanes, especially CH_4, to high-valued liquid alkanes. We have shown that disordered Ru clusters have better activity and selectivity in the reaction than rigid particles,[26] but the structure-function relationship needs further understanding for the rational design of active sites. For hydrocracking, most studies used expensive, scarce Pt as the metal,[27-34] and zeolites as the acidic support,[30-35] the microporous structure of which creates difficulty for the diffusion of long-chain polymers and thus limits active site accessibility. Also, mechanistic understanding is very rare,[27] which hinders tuning product distribution rationally. Furthermore, there are no studies of the two reactions occurring simultaneously, which is common on bifunctional catalysts with small alkanes.[10] This type of studies do not only help understand the complex reaction network, also offer insights on how to choose between the processes and design catalyst functionality.

In this work, we investigated the hydrogenolysis and hydrocracking of PP, LDPE, and model alkanes that co-occur on a low-loading Ru/TiO_2 catalyst. Ni/TiO_2 was also studied for hydrocracking as a noble-metal-free catalyst. We show that the superior activity and selectivity of hydrocracking to hydrogenolysis make the bifunctional Ru/TiO_2 more suitable than monofunctional Ru catalysts for PP conversion. Lower hydrogen pressure and more branched products increase the tendency for the reaction to occur through hydrocracking, which can also be effectively catalyzed by Ni/TiO_2. The unexpected bifunctionality of Ru/TiO_2 was attributed to auto-adsorbed carboxylates on TiO_2. This work elucidates the co-existence of the two routes on a bifunctional catalyst, the relationship and comparisons between them, and how the mechanism of polyolefin upcycling is altered by reaction conditions and catalysts. Also, the results on the Brønsted acidity of TiO_2 opens brand new opportunities in developing novel acid catalysts.

Results

1. *Unique performance of an anatase TiO_2 support in PP conversion over low-loading Ru*

We previously discovered that decreasing Ru loading on CeO_2 to a threshold triggers an increase in the disorder in the Ru structure, which coincides with drastic increases in the activity, selectivity, and isomerization ability in polyolefin hydrogenolysis.[26] This discovery motivated us to examine how the support regulates the properties and thus performance of highly dispersed Ru species. Therefore, we impregnated low-loading Ru (0.07 Ru/nm^2) onto various supposedly non-acidic supports (see Table S1 for BET surface area), and tested them in the hydrogenolysis of PP and LDPE (260 °C, 30 bar H_2). Results are summarized in Figure 1, with the best catalyst studied from previous works, Ru/CeO_2, as a reference point.[26] Surprisingly, an anatase TiO_2 synthesized by a sol-gel method[36] (referred to as "TiO_2-A-SG", XRD see Figure S1a) clearly stands out with PP as the substrate (Figure 1a), showing by far the best per-Ru conversion rate (~350 g_{PP} g_{Ru}^{-1} h^{-1}, patterned bar, 3 times as high as Ru/CeO_2), selectivity (< 5% CH_4, green, ~80% liquid products, purple), and isomerization ability (> 60% isomers, orange). Nevertheless, its activity and selectivity with LDPE as the substrate is mediocre (Figure 1b), except for the high fraction of branched products (red). Meanwhile, among other supports, the performance of low-loading Ru is highly support-dependent with both PP and LDPE, and particularly, they surprisingly exhibit negligible activity on two supports, commercial anatase TiO_2, ("TiO_2-A-comm"), and carbon. This manuscript will only present detailed studies to understand the unique, intriguing performance of the TiO_2-A-SG support. The strong support-dependence among other catalysts was hypothesized to be due to different morphology of highly dispersed Ru species, which we will report in a separated manuscript.

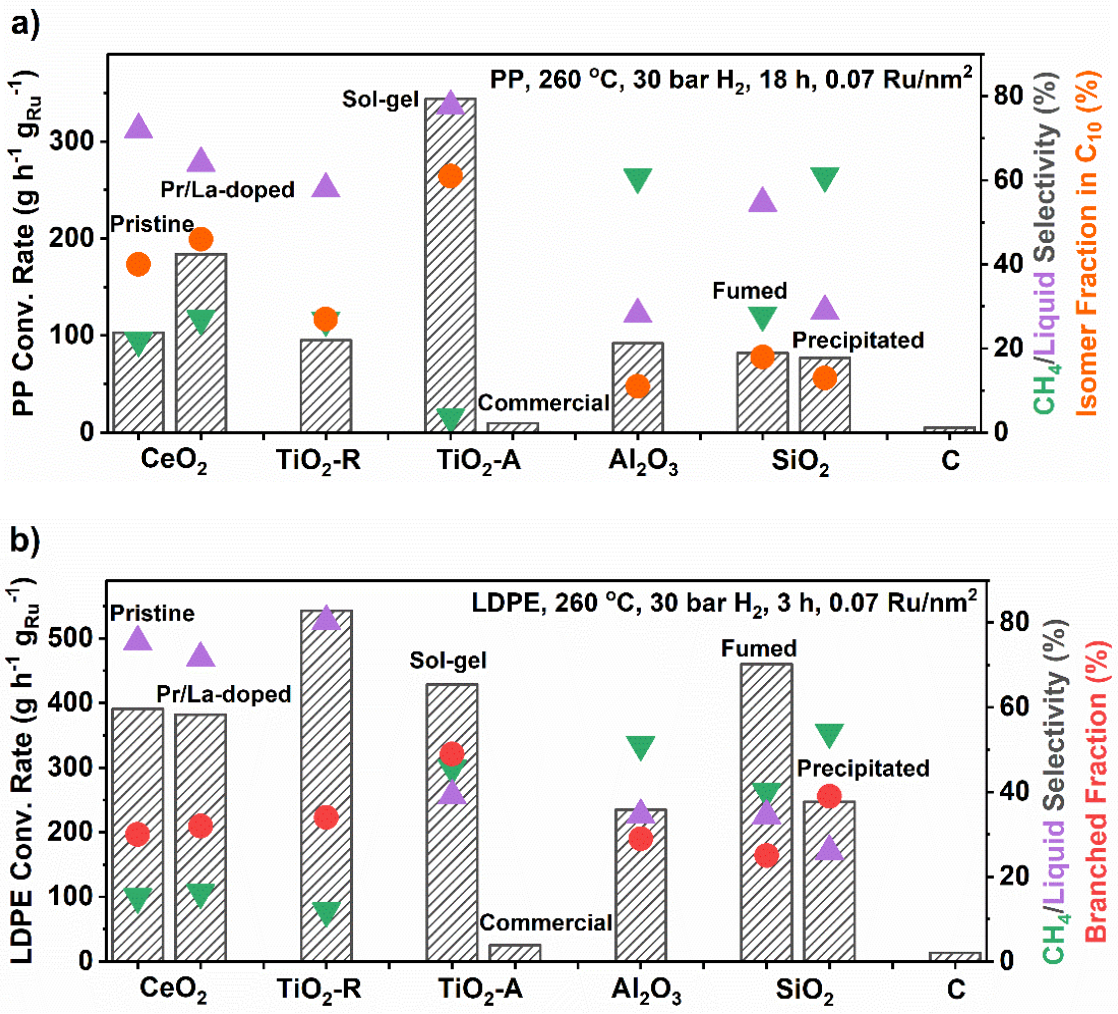

Figure 1. Performances of low-loading Ru (0.07 Ru/nm^2) on various supports in the upcycling of **a)** PP and **b)** LDPE at 260 °C under 30 bar H_2. Patterned bars represent the per-Ru conversion rate of the polymer solid (left *y*-axis). For right *y*-axis, green and purple traingles repersent the selectivity towards CH_4 and liquid products, respectively. Orange dots in panel a) represent the fraction of isomerized products in all C_{10} products. Red dots in panel b) represent the fraction of branched products in $C_{12\text{-}22}$ products. Catalyst with 0.5 mg Ru was used in each reaction. Another set of experiments with lower Ru loading shows similar results (Table S2).

2. *Bifunctional Ru/TiO_2-A-SG catalyzing both hydrocracking and hydrogenolysis*

We noticed that besides the high activity, low CH_4 selectivity, and good isomerization ability, Ru/TiO_2-A-SG also exhibits unique product distribution characteristics in PP upcycling. Figure 2b shows the product distribution typical for PP hydrogenolysis over other Ru catalysts,

with Ru/CeO_2 as the example. It has abundant C_{2-3} besides CH_4, and wide distribution among liquid products centered around C_{22}, while both liquid products and solid residue have no color.[13] In contrast, Figure 2c shows that Ru/TiO_2-A-SG generates abundant C_{4-5} with minimal C_{2-3}, the liquid products have a much narrower distribution centered around C_{10}, and both liquid products and solid residue are light yellow (Figures S2a and S2e).

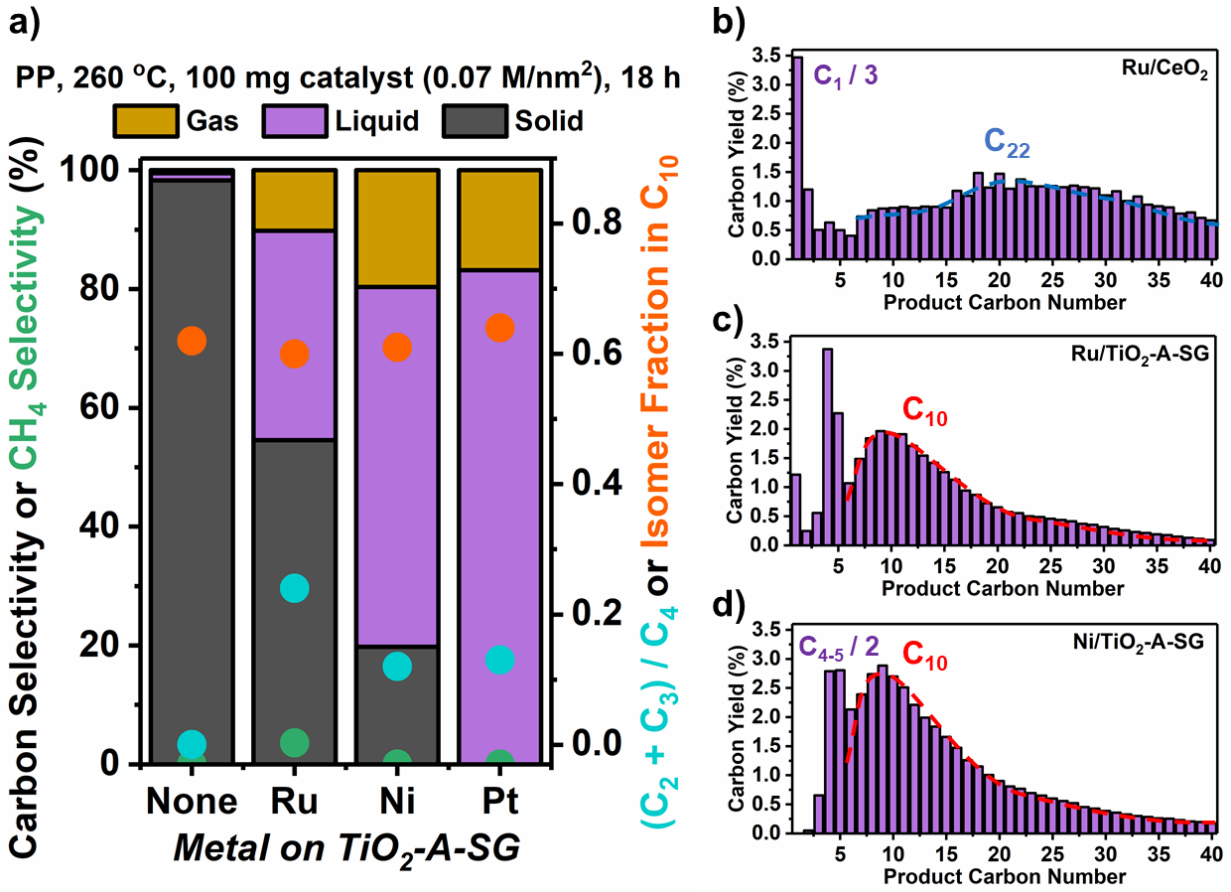

Figure 2. Panel **a)** shows the performance of various types of metals on the sol-gel anatase TiO_2 (TiO_2-A-SG) support (0.07 M/nm^2) in PP upcycling under 30 bar H_2. Black, purple, and yellow bars represent carbon selectivity, i.e., the fraction of quantifiable C in solid, liquid, and gas phases after the reaction (left *y*-axis). Greend dots represent the CH_4 selectivity (left *y*-axis). Cyan dots represent the $(C_2 + C_3) / C_4$ value, i.e., the ratio between C_{2-3} yields, and C_4 yield (right *y*-axis). Orange dots represent the fraction of isomerized products in all C_{10} products. Panels **b)** – **d)** show carbon yields of C_{1-40} products over Ru/CeO_2, Ru/TiO_2-A-SG, and Ni/TiO_2-A-SG, repsectively. In panel b), C_1 yield was plotted with 1/3 of its value. In panel d), C_{4-5} yields were plotted with half of their values.

Since the high isomerization level and the lack of C_{1-2} products are typical characteristics for alkane hydrocracking,[10, 27, 29, 37-40] we suspect that Ru/TiO_2-A-SG converts PP mainly through hydrocracking, instead of hydrogenolysis. In hydrocracking, C−C bonds are cleaved on Brønsted acid sites (BAS), and the metal only needs to catalyze dehydrogenation/hydrogenation.[10] Thus, to test the hypothesis, we impregnated Ni and Pt onto TiO_2-A-SG (0.07 M/nm^2), both of which are inert for C−C bond cleavage, i.e., hydrogenolysis, under these conditions.[12, 13, 26] Figure 2a shows that both Ni and Pt convert PP on TiO_2-A-SG more efficiently than Ru, yielding similar product distribution (Figures 2d and S3b): no CH_4, much more C_{4-5} than C_{2-3}, narrow liquid distribution around C_{10}, and yellow-colored products (Figure S2f). In addition, the TiO_2-A-SG support alone, without any metal, can convert ~5% PP (Figure 2a), also with similar product distribution (Figure S3c). These results confirm that M/TiO_2-A-SG can convert PP through hydrocracking, in which C−C bond cleavage occur on TiO_2-A-SG, while the metal facilitates (de)hydrogenation steps. The presence of the more selective hydrocracking pathway on Ru/TiO_2-A-SG explains its unique performance in PP upcycling in Figure 1a. Since the two pathways on M/TiO_2-A-SG exhibit very different selectivity between C_{4-5} and C_{2-3}, we use the ratio between C_{2-3} yields and C_4 yield (referred to as "(C_2 + C_3) / C_4", cyan in Figure 2a, C_5 hard to quantify due to the high vapor pressure) as a reaction pathway indicator, along with the CH_4 selectivity. For hydrogenolysis-only reactions on all Ru catalysts we have studied,[13, 26] this value is > 2.0 (Table S3 and Figure S4), which would significantly decrease if hydrocracking also occurs.

The obvious question here is why TiO_2-A-SG can catalyze C−C bond cleavage, as TiO_2 is not expected to have BAS required for it. Therefore, we impregnated Ni onto various oxides (0.07 Ni/nm^2 if not specified), and tested them in PP upcycling under the same conditions to verify that the second pathway is hydrocracking. Table 1 shows that Ni only converts PP and

forms yellow solid residues on supports known for having BAS, i.e., Nb_2O_5 and SSZ-13 zeolite (entries 4-6),[41-43] while other supports showing relatively good PP upcycling performance with Ru in Figure 1a, i.e., CeO_2, rutile TiO_2, "TiO_2-R" and fumed SiO_2, do not convert PP with Ni (entries 1-3). These results further support that the superior performance of Ru/TiO_2-A-SG in Figure 1a is due to its unique bifunctionality that enables hydrocracking. Hydrocracking allows efficient PP conversion using non-noble metals with good (de)hydrogenation ability, such as Ni, another advantage over hydrogenolysis besides the desired selectivity. We note that TiO_2-A-SG is a particularly effective acidic support for PP hydrocracking, showing higher activity than SSZ-13 with even 10 times Ni loading (entry 7 compared to 6). This could be due to the absence of micropores on TiO_2-A-SG (Figure S1b) causing less diffusion limits of the long-chain polymers.

Table 1. Activity of Ni supported on various oxides in the hydrocracking of PP.

Entry	Support (0.07 Ni/nm^2)	Post-synthesis history	PP conversion (%)	Residual yellow?
1	TiO_2-R	RT air 1 day	< 1	No
2	CeO_2		< 1	No
3	SiO_2-fumed		< 1	No
4	Nb_2O_5	RT air 1~3 days	5	Yes
5	SSZ-13 [a]		23	Yes
6	SSZ-13-10Ni [b]		51	Yes
7	TiO_2-A-SG-B1	RT air 2 months	88	Yes
8		RT air 1 day	22	Yes
9		RT air 3 weeks	46	Yes
10	TiO_2-A-SG-B2 [c]	RT air 3 weeks, Calcination [d]	< 1	No
11		Acetic acid exp. [e]	57	Yes
12		Acetic acid exp., Calcination	< 1	No

[a] Si : Al = 6, synthesized in-house,[44] NH_4^+ exchanged, calcined before Ni impregnation.
[b] Ni surface density on this catalyst is 10 times of other catalysts (0.7 Ni/nm^2).
[C] This sample uses a second batch of TiO_2-A-SG synthesized following the same procedure.
[d] Calcination was performed at 500 °C for 4 h before the reaction (~5 min air exposure in between).
[e] Acetic acid exposure was performed using the procedure described previously after 3 weeks RT air exposure.[45]

Since TiO_2 surfaces were known to auto-adsorb ppm-level formic/acetic acids in the air to form mixed carboxylate layers,[45-47] we suspected that the unexpected BAS on TiO_2-A-SG are associated with these chemisorbed layers. M/TiO_2-A-SG were calcined at 400 °C for 4 h in the final step of the synthesis. This step would remove the carboxylic layers,[45] which re-accumulate during the storage (Figure S5 mid showing their presence after long-term storage by C 1*s* XPS). Thus, we controlled the post-synthesis history of Ni/TiO_2-A-SG to test the hypothesis. Table 1 shows that the PP conversion on Ni/TiO_2-A-SG increases with longer post-synthesis air exposure at room temperature (entries 8-9), and drops to ~0 after calcining the catalyst again before the reaction (entry 10). The results indicate that the BAS on TiO_2-A-SG are formed by contacting air at room temperature, and removed by high-temperature calcination, aligning well with the behaviors of the carboxylate layers on TiO_2 surfaces.[45] We also exposed Ni/TiO_2-A-SG to acetic acid vapor to saturate TiO_2 surfaces with the layers, which increases the PP conversion (entry 11 compared to entry 9), further supporting the hypothesis. We note that after the acetic acid vapor exposure, the catalyst also carries a significant amount of physisorbed acetic acid (reflected by the significant mass increase and strong smell). The fact that the PP conversion increase caused by it is not significant (46% to 57%) indicates that the chemisorbed carboxylate layers are much more active in PP hydrocracking than physisorbed acetic acid. Calcining acetic-acid-saturated Ni/TiO_2-A-SG still eliminates its hydrocracking activity, i.e., BAS on it, as we expected (entry 12). Overall, the control experiments strongly imply that the BAS on TiO_2-A-SG originate from the carboxylates it adsorbs from the air. We will discuss the carboxylate layers and BAS in more details in the Discussions section.

3. Effects of P_{H2} and competition between the two pathways

The fact that Ru/TiO_2-A-SG does show slightly higher CH_4 selectivity and (C_2 + C_3) / C_4 value in Figure 2a (3.6% and 0.24) than Ni and Pt (0% and ~0.16) indicates that on Ru/TiO_2-A-SG, hydrogenolysis occurs to a minor extent alongside hydrocracking. Thus, we investigated the contribution of the two pathways under different H_2 partial pressure (P_{H2}). Figure 3a shows that the CH_4 selectivity remains < 5% at $P_{H2} \leq 30$ bar, but increases abruptly to > 20% at ≥ 45 bar. A similar trend was observed for the (C_2 + C_3) / C_4 value (< 0.3 at ≤ 30 bar, ~1 at 45 bar) as well. For hydrogenolysis over monofunctional Ru catalysts, when P_{H2} increases, the CH_4 selectivity always decreases because the cleavage of terminal C−C bonds involves more dehydrogenated transition states (TS) than that of internal C−C bonds, and the more facile product desorption suppresses sequential C−C bond cleavage that favors CH_4 formation,[13, 26] while the (C_2 + C_3) / C_4 value also decreases in all our studies (Figure S4). Therefore, the increase in both values at high P_{H2} cannot be explained by regioselectivity shifts in hydrogenolysis. Instead, it reflects the transition from a low-P_{H2} regime, in which hydrocracking dominates, to a high-P_{H2} regime, in which the contribution from hydrogenolysis is significant. This is consistent with the changes in liquid product distribution, from a narrow distribution around $C_{10–12}$ with yellow color at ≤ 30 bar (Figures 2b and S3f-g), to a wide double distribution around $C_{10–12}$ and C_{18} with no color at ≥ 45 bar (Figures 2c and S3j). In the high-P_{H2} regime, the isomerization level remains at ~60%, which, along with the double liquid distribution, indicates that both pathways have significant contribution to the reaction. The shift in the prevailing pathway with P_{H2} suggests that the rate of hydrocracking is less sensitive to P_{H2} than that of hydrogenolysis. As a result, the bifunctional Ru/TiO_2-A-SG converts PP much more effectively at low P_{H2} than most active monofunctional Ru catalysts (223 g_{PP} g_{Ru}^{-1} h^{-1} at 5 bar, Figure 3a, compared to ~30 g_{PP} g_{Ru}^{-1} h^{-1} on Ru/CeO_2[26]).

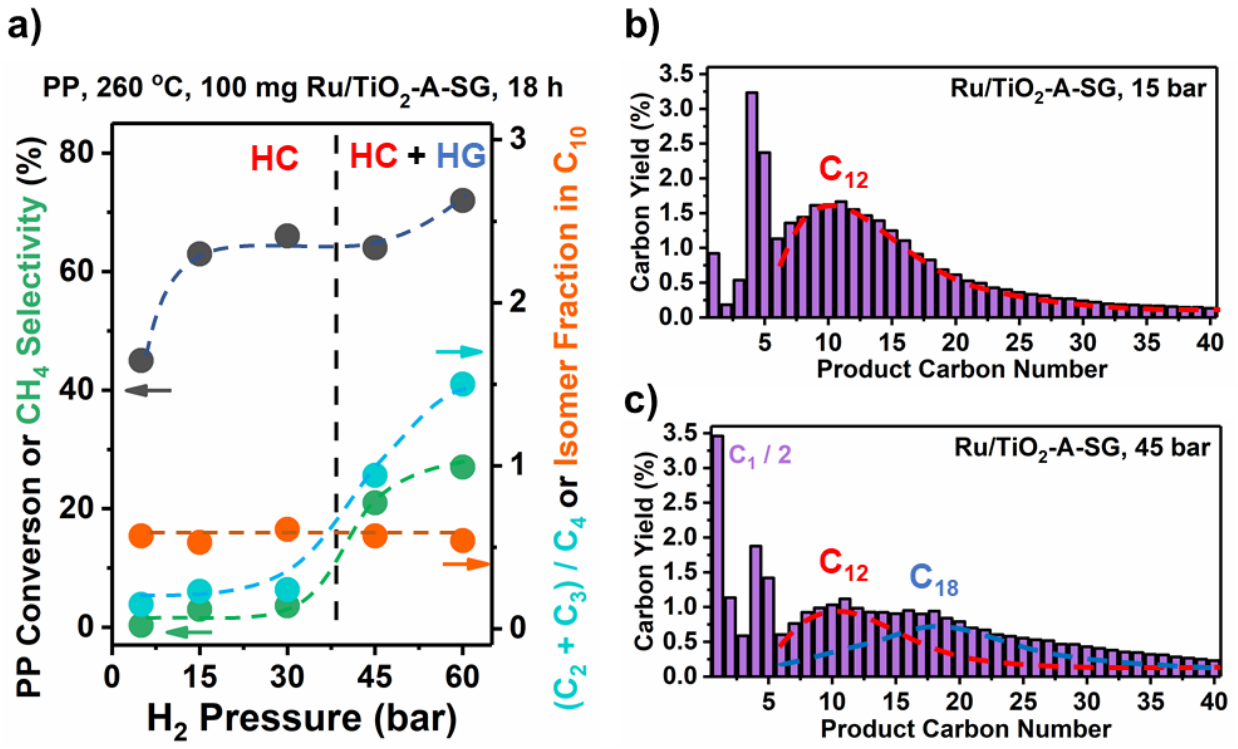

Figure 3. Effects of hydrogen partial pressure (P_{H2}) on the performance of Ru/TiO_2-A-SG in PP upcycling. Panel **a)** shows variations in the PP conversion (black, left *y*-axis), CH_4 selectivity (green, left *y*-axis), (C_2 + C_3) / C_4 (cyan, right *y*-axis), and the fraction of isomerized products in C_{10} (orange, right *y*-axis) with P_{H2}. Panels **b)** and **c)** show a representative example of product carbon distribution in the low- (≤ 30 bar) and high-P_{H2} (≥ 45 bar) regime, respectively. Product carbon distribution from all experiments can be found in Figure S3.

Interestingly, when P_{H2} increases from 15 to 45 bar, the PP conversion remains constant (Figure 3a) while the hydrogenolysis rate increases (reflected by higher C_1 – C_3 yields, Figures S3g-i), indicating that the rate of hydrocracking decreases as P_{H2} increases. In hydrocracking, alkanes are dehydrogenated on the metal, resulted alkenes are transported to BAS, isomerized and cracked through C^+ intermediates, and then transported back to the metal for hydrogenation (Scheme 1).[10] Since TiO_2-A-SG does not have shape selectivity effect from micropores (Figure S1b),[37] the high C_{4-5} yields in Figures 2c-d suggest severe secondary cracking before desorption. Also, the formation of C_3 from PP indicates appreciable C−C bond cleavage through type-B *β*-

scissions. Both observations suggest that on Ru/TiO_2-A-SG, the alkane dehydrogenation step is not equilibrated (see the Discussions section for detailed mechanistic explanations),[10] which is not surprising with the low metal loading. In this situation, the consumption of dehydrogenated intermediates on Ru (in the purple box in Scheme 1) through hydrogenolysis, i.e., C−C bond cleavage,[13, 48, 49] reduces the amount of them desorbing as alkenes. The faster hydrogenolysis at higher P_{H2} thus decreases free alkene concentrations in the system, suppressing hydrocracking. The conclusion is further supported by Table S4, which shows that doubling Ru loading on TiO_2-A-SG does not increase the PP conversion but makes the product distribution more resemble hydrogenolysis (Figures S3d and S3e compared to Figures S3h and S3f, respectively), i.e., higher Ru loading leads to slower hydrocracking. Since the alkane dehydrogenation step over Ru is not equilibrated, more Ru would increase hydrocracking rate if hydrogenolysis did not interfere with it. Thus, the lower hydrocracking rate reflects that it is suppressed by the faster hydrogenolysis on larger Ru particles.[50, 51]

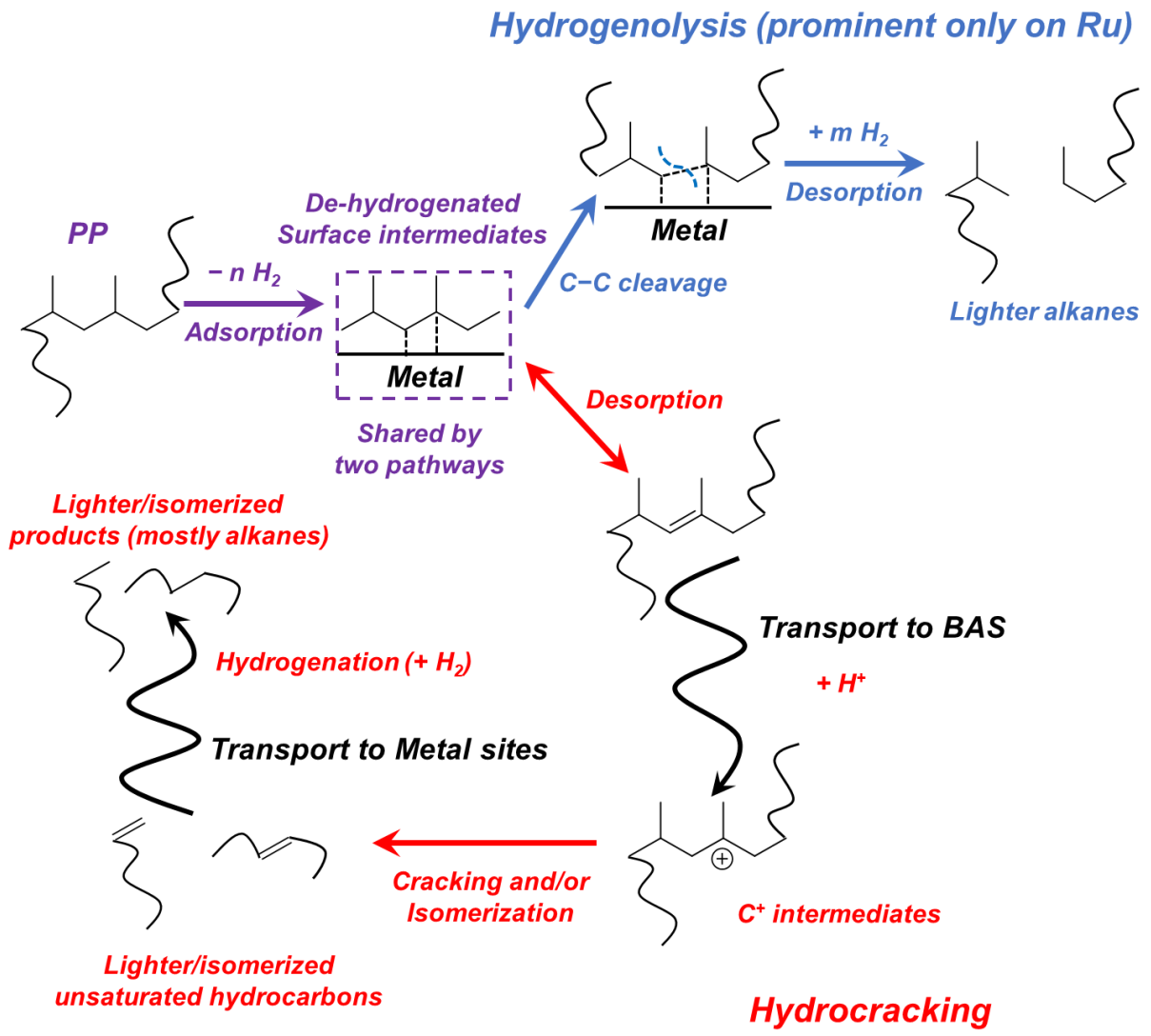

Scheme 1. Mechanistic scheme of the dual-pathway PP upcycling over M/TiO_2-A-SG catalysts.

4. Relative importance of the two pathways dependent on the substrate branching level

We have demonstrated the co-existence of hydrocracking and hydrogenolysis pathways in the PP conversion on bifunctional Ru/TiO_2-A-SG, which brings the question of whether the dual-pathway scheme is applicable to other less branched substrates. Thus, we compared the reaction of four substrates with various branching levels (quantified by the fraction of ^3C in total C, *n*-$C_{16}H_{34}$, no ^3C; LDPE, ~ 2% ^3C,[52] squalane, structure see Scheme 2a, 20% ^3C, and PP, 33%

^{3}C) on Ni/TiO_2-A-SG at 30 bar, and on Ru/TiO_2-A-SG at 5 and 30 bar. Ni/TiO_2-A-SG converts all substrates, yielding no $C_{1\text{-}2}$, minimal C_3, and high fraction of isomers (Table 2 and Figure S6), indicating that hydrocracking is present with all substrates. Since hydrogenolysis is not catalyzed by Ni and its rate is more sensitive to P_{H2} than that of hydrocracking, we used two parameters: 1) the ratio between the rate on Ni and Ru at 30 bar, and 2) the ratio between the rate on Ru at 5 bar and 30 bar, to gauge the relative importance of the two pathways. Table 2 and Figure S7 show that increasing substrate branching level leads to increases in both indicators, i.e., the relative importance of hydrocracking to hydrogenolysis. The conclusion is also supported by the lower (C_2 + C_3) / C_4 value with more branched substrates under identical conditions on Ru (Table 2 and Figure S7). It is expected based on previous studies with small-alkanes, as 1) hydrocracking mainly proceeds through $^{3}C^{+}$ intermediates (type-A β-scissions), and less branched substrates require more extensive isomerization prior to C−C bond cleavage,[10] and 2) ^{3}C–^{x}C bonds are less reactive than ^{2}C–^{2}C and ^{2}C–^{1}C bonds in hydrogenolysis due to their high steric hindrance limiting the ability to access the most stable TS.[48, 49]

Table 2. Results of the reaction of various alkanes over M/TiO_2-A-SG catalysts.

Substrate (^{3}C frac.)	Metal	P_{H2} (bar)	Conv. (%)	r(Ni) : r(Ru) at 30 bar	r(5 bar) : r(30 bar) on Ru	S_{CH4} (%)	(C_2 + C_3) / C_4
n-$C_{16}H_{34}$ (0)	Ni	30	0.7	0.05	N/A	0	0.1
	Ru	30	14		0.18	23	2.9
		5	2.6			15	2.1
LDPE (~0.02)	Ni	30	7.0	0.28	N/A	0	0
	Ru	30	25		0.18	45	4.7
		5	4.5			30	2.0
Squalane (0.2)	Ni	30	7.4	0.65	N/A	0	0
	Ru	30	11		0.48	8.0	2.6
		5	5.4			3.0	1.0
PP (0.33)	Ni	30	88	1.44	N/A	0	0
	Ru	30	61		0.60	3.6	0.24
		5	37			0.3	0.15

Reaction condition: 260 °C, 1 g substrate, *m*(catalyst) and reaction time as following: *n*-$C_{16}H_{34}$ – 8 mg, 3 h; LDPE – 50 mg, 3 h; squalane – 8 mg, 3 h; PP – 100 mg, 18 h.

Reactions of linear substrates, i.e., LDPE and *n*-$C_{16}H_{34}$, on Ru/TiO_2-A-SG were studied over the entire P_{H2} range to further understand them. Figures 4a-b show that at ≥ 15 bar, both reactions follow typical hydrogenolysis behaviors previously reported and attributed to changes in *H coverage: as P_{H2} increases, the rate increases then decreases, while the CH_4 selectivity, (C_2 + C_3) / C_4, and branched alkane fraction from LDPE decrease motonously.[13, 26] Hydrocracking characteristics such as low CH_4 selectivity and (C_2 + C_3) / C_4, as well as high isomerization level (analyzed with *n*-$C_{16}H_{34}$, Figure 4b), were observed only at 5 bar, indicating that with the linear substrates, hydrocracking is only important at very low P_{H2} (5 bar). Even at P_{H2} = 5 bar, both CH_4 selectivity and (C_2 + C_3) / C_4 are significantly higher than the values in hydrocracking over

Ni/TiO_2-A-SG in Table 2, suggesting that hydrogenolysis remains significant. In comparison, hydrocracking exhibits absolute prevalence with PP at ≤ 30 bar (Figure 3a), further emphasizing that hydrocracking is more favored with more branched substrates. The substrate-dependence of the two pathways explains why in Figure 1b, the bifunctionality of Ru/TiO_2-A-SG does not lead to superior performance in LDPE upcycling: the contribution of hydrocracking is minimal with LDPE, and Ru/TiO_2-A-SG has mediocre activity/selectivity in hydrogenolysis (will be shown in detail in a separated manuscript). We note that Ru/TiO_2-A-SG yields higher fraction of branched alkanes from LDPE than other Ru catalysts with similar CH_4 selectivity, but the regioselectivity of hydrogenolysis predicts the two parameters to move in sync.[13, 26, 53] This is because branched alkanes can also be produced on Ru/TiO_2-A-SG by isomerization on BAS.

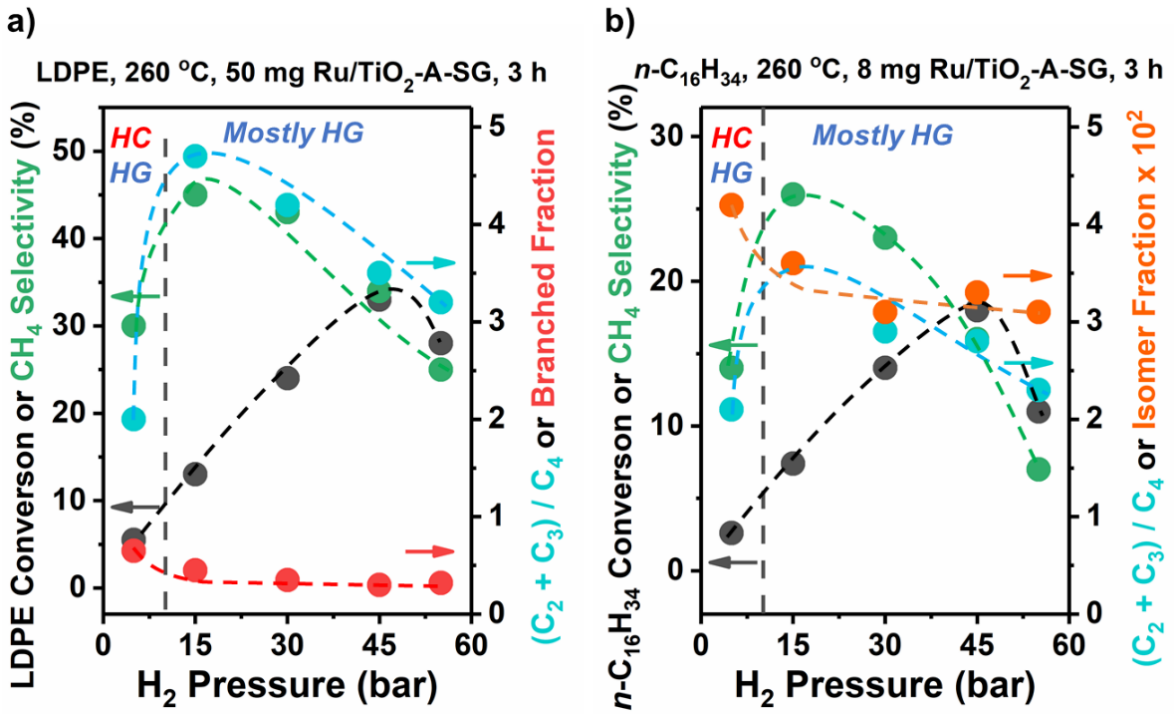

Figure 4. Effects of hydrogen partial pressure (P_{H2}) on the performance of Ru/TiO_2-A-SG in the reaction of **a)** LDPE and **b)** *n*-$C_{16}H_{34}$. Black, green, and cyan dots show the substrate conversion (left *y*-axis), CH_4 selectivity (left *y*-axis), and (C_2 + C_3) / C_4 (right *y*-axis), respectively. Red dots in panel a) represent the fraction of branched products from LDPE, while orange dots in panel b) represent the fraction of branched alkanes from *n*-$C_{16}H_{34}$, which gauges the isomerization level.

The close examination of C_{10} products from squalane offers further mechanistic insights. Table 3 shows that on Ru/TiO_2-A-SG at 30 bar, 75% of the C_{10} products are non-isomers (see discussions related to Figure S8 for analysis details), indicating that hydrogenolysis is the main pathway under such conditions. Meanwhile, the absolute majority of non-isomerized products are dimethyloctanes, which are produced by cleaving only $^{2}C–^{2}C$ bonds (blue in Scheme 2b), rather than methylnonanes, the formation of which requires cleaving at least one $^{3}C–^{x}C$ bonds (red in Scheme 2b). Considering that isomerization is insignificant, the observation indicate that in hydrogenolysis, the cleavage of $^{2}C–^{2}C$ is strongly favored over that of $^{3}C–^{x}C$ bonds, aligning well with the literature of small-alkane hydrogenolysis.[48, 49] In comparison, on Ni/TiO_2-A-SG or at 5 bar, significantly more isomers are produced, supporting that decreasing P_{H2} or replacing Ru with the hydrogenolysis-inactive Ni shift the reaction pathway towards hydrocracking.

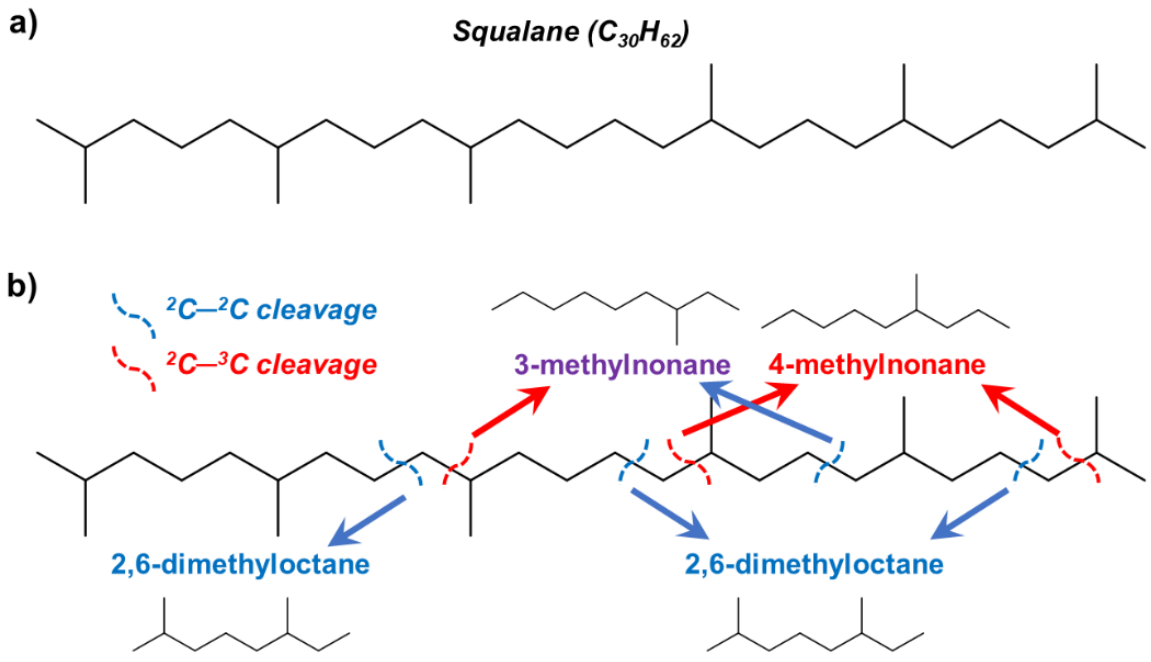

Scheme 2. Drawing **a)** shows the structure of squalane. Drawing **b)** shows examples of C–C bond cleavage required to produce dimethyloctanes and methylnonanes from squalane with no isomerization. Blue and red represent the cleavage of $^{2}C–^{2}C$ and $^{2}C–^{3}C$ bonds, respectively. Other ways to produce these compounds exist, but the type of C–C bonds that need to be cleaved is identical with examples shown here (see Figure S8 and related discussions for details).

Table 3. Distribution of C_{10} products from squalane on M/TiO_2-A-SG catalysts.

Metal, P_{H2} [a]	Non-isomer fraction [b]	Dimethyloctanes : Methylnonanes
Ru, 30 bar	75%	49
Ru, 5 bar	34%	25
Ni, 30 bar	10%	N/A

[a] Reaction conditions are identical with Table 2.
[b] "Non-isomers" include dimethyloctanes and methylnonanes.

Discussions

1. *Comparing hydrocracking with hydrogenolysis on M/TiO_2-A-SG and mechanisms*

Our results demonstrated the two pathways of polyolefin conversion on the bifunctional Ru/TiO_2-A-SG: hydrocracking and hydrogenolysis. Compared to hydrogenolysis, hydrocracking has several advantages. First, it produces minimal low-valued C_{1-3} products (Figure 2d). C−C cleavage in hydrocracking is mainly achieved through two types of β-scissions: type-A, which starts and ends both with a $^3C^+$, and type-B, which starts or ends with one $^2C^+$ (Scheme 3).[10, 27, 37-40] C_{1-2} are absent because the $^1C^+$ intermediates involved in their formation are too unstable.[10] C_3 yield is low because only type-B β-scissions at the chain ends can produce C_3 (Scheme 3), which are much slower than type-A β-scissions.[37-40] Besides, at the chain ends of virgin PP, primary β-scissions always start with $^3C^+$, and thus there are no type-B1 β-scissions (Scheme 3). In contrast, primary C−C bond cleavage in hydrogenolysis does not discriminate against C_{1-3}, and sequential C−C cleavage, if the desorption is slow, favors CH_4 formation.[50, 51, 54] Second, hydrocracking is more suitable for low-P_{H2} operation. When P_{H2} decreases from 30 to 5 bar, the PP conversion drops much less significantly on the bifunctional Ru/TiO_2-A-SG (37% drop in Figure 3a) than on monofunctional Ru catalysts (70%, 80%, and 75% on 0.125%, 2% Ru/CeO_2,[26] and 5% Ru/C,[13]

respectively), and the former converts PP at least 7-fold faster at 5 bar. Third, hydrocracking is accompanied by isomerization, producing more branched alkanes from LDPE (Figure 1b) and likely aromatics (implied by the yellow color of products). Fourth, hydrogenolysis requires noble metals (Ru, Rh, or Pt with polyolefin substrates),[13, 15] while the non-noble metal Ni can catalyze hydrocracking even more efficiently than Ru (Figure 2a).

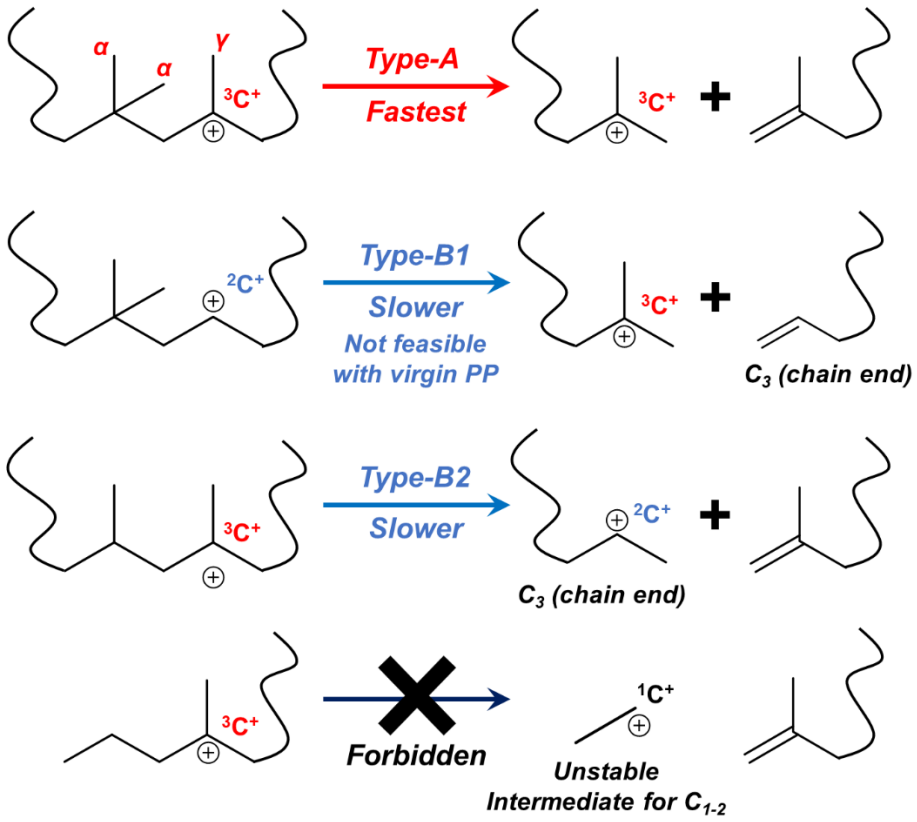

Scheme 3. Different types of *β*-scissions in hydrocracking and intermediates involved.

Despite the superior efficiency and selectivity with PP, hydrocracking on Ni/TiO_2-A-SG is not as effective as hydrogenolysis on Ru/TiO_2-A-SG with less branched substrates (Table 2), as the virgin structure with minimal ^{3}C requires extensive isomerization before *β*-scissions,[10] and has less steric hindrance for hydrogenolysis.[49] Thus, hydrogenolysis might be more suited for the upcycling of PE, particularly HDPE. Another undesired feature of PP hydrocracking on M/TiO_2-

A-SG is the strong tendency to produce C_{4-6} (Figure 2d, observed at low PP conversion as well, Figure S9, C_6 yield underestimated due to the fast evaporation). The high C_{4-6} yields on non-microporous catalysts are signs of significant secondary cracking, i.e., consecutive β-scissions before desorption, which will stop when the substrate does not have 7 C atoms (Scheme 3).[10, 37, 40] This usually occurs because the dehydrogenation ability of the catalyst is too low to establish the alkane/alkene equilibrium, leading to low free alkene concentration that cannot displace products from BAS.[10] Replacing Ni with Pt, which has better dehydrogenation ability, enhances the rate (Figure 2a), confirming that on Ni/TiO_2-A-SG, dehydrogenation is the slow step. This also increases chances for type-B β-scissions and thus C_3 formation. Type-A β-scissions require three branches in the α, α, γ-configuration (Scheme 3),[10, 37-40] which is absent in virgin PP/LDPE. Therefore, isomerization is required prior to type-A β-scissions,[10, 40] which was known to be favored by high free alkene concentration.[27] The weak dehydrogenation ability is caused by the low metal loading (0.07 M/nm^2), and one should be able to alleviate the problem and shift the selectivity towards higher-valued heavier products by increasing the metal loading. In Figure S3, Pt/TiO_2-A-SG yields less C_{3-6} than Ni/TiO_2-A-SG despite higher PP conversion, confirming that enhancing the dehydrogenation ability suppresses the formation of these light products.

As for less branched substrates, hydrocracking on Ni/TiO_2-A-SG also generates no C_{1-2} products (Figure S6, for the same reason with PP), but less C_{4-6}. This could be explained as these substrates have less ^{3}C with high steric hindrance, leading to faster dehydrogenation, higher free alkene concentration, and thus less secondary cracking. We note that LDPE and *n*-$C_{16}H_{34}$ both have ^{2}C at chain ends in the virgin structure, which allows type-B1 β-scissions. C_3 yields are still low, suggesting that the isomerization – type-A β-scission sequence is preferred over type-B β-scission, consistent with the literature.[10, 27, 37-40] We also noticed that in the hydrocracking of PP

(on Ni/TiO_2-A-SG), the hardness of the solid residue does not seem to change with the PP conversion. This echoes with previous report that the average M_W (GPC-based) of the solid does not decrease significantly with hydrocracking reaction time,[27] and implies that hydrocracking preferentially converts smaller products over large polymers, opposite of hydrogenolysis.[13, 26] This could be due to the secondary cracking, which is enhanced by the mass transfer limitation in the viscous environment trapping products around BAS and causing re-adsorption, and/or the slower diffusion of large polymers preventing it to reach BAS after dehydrogenation.

2. Origin and implications of the Brønsted acidity of TiO_2-A-SG

Another intriguing result from this work is the unexpected Brønsted acidity of TiO_2-A-SG associated with the carboxylate layers auto-adsorbed from the air (Table 2). It has long been known in surface science studies that hydrocarbon layers are formed under air on TiO_2, altering its surface properties.[46, 55] The chemical identity of the layers was recently elucidated as mixed formate/acetate, formed by the strong dissociative adsorption of formic/acetic acids ubiquitously present in the air at ppm levels.[47, 56] They are removed by UV radiation or H_2/air at ≥ 350 °C,[45, 56] but stable during laboratory storage, and their presence is detected by XPS (Figure S5) and IR as shown in our previous work.[45] TiO_2 is widely used in thermo-catalysis as the catalyst or the support, and it is not always treated *in-situ* at high temperature prior to the reaction. Nevertheless, effects of the carboxylate layers in thermo-catalysis have been ignored, until we recently reported that they can poison Pt/Al_2O_3 catalysts in CO_2 hydrogenation by blocking formate formation sites.[45] This work is, to our knowledge, the first demonstration that they can add functionality, i.e., Brønsted acidity, to a catalyst.

We believe that certain requirements exist for the carboxylate layers on TiO_2 to exhibit Brønsted acidity. All three types of TiO_2 we tested have the carboxylate layers (Figure S5), but only TiO_2-A-SG shows hydrocracking activity. Rutile, or even anatase from the commercial source do not. The observations resonate with our previous report that the layers on TiO_2-A-comm deactivate Pt/Al_2O_3 in CO_2 hydrogenation while those on TiO_2-R do not. We propose two possible structures of the BAS on TiO_2-A-SG: 1) the surface −OH formed along with the carboxylates in the dissociative adsorption of acids;[47] 2) the re-protonation of carboxylates under reaction conditions (≥ 5 bar H_2, 260 °C). Because physisorbed acetic acids are much less active for PP hydrocracking than the chemisorbed carboxylate layers (Table 2), we suggest that the first possibility is more likely. Regardless, the properties of the carboxylate layers should be sensitive to the strength and configuration of their chemisorption, which vary with the properties of TiO_2. This would impact their catalytic behaviors, such as Brønsted acidity or deactivating Pt/Al_2O_3,[45] leading to the varying results among the three TiO_2. We also note that three batches of TiO_2-A-SG were synthesized for this work, which all exhibit hydrocracking activity with Ni, but the rate varies to a minor extent (two batches shown in Table 2, the third batch between them). This could be due to the subtle structural difference among the batches in surface area, exposed facets, and/or defects. This novel discovery invokes complicated questions on the structure and property of the carboxylate layers and BAS on TiO_2, which are fundamentally intriguing and practically appealing as they can serve as a new type of Brønsted-acid catalysts under proper conditions for reactions beyond polyolefin hydrocracking. While this work focuses on polyolefin upcycling over M/TiO_2-A-SG, we will attempt to address these questions with more detailed spectroscopic studies and simpler probe reactions in the future.

Conclusions

In this contribution, we report that low-loading Ru on a sol-gel anatase TiO_2 (TiO_2-A-SG) can upcycle polyolefin into small hydrocarbons under H_2 through hydrocracking, in addition to hydrogenolysis that is common on Ru catalysts. Compared to hydrogenolysis, hydrocracking shows more desired product selectivity in minimal low-valued C_{1-3}, liquids with narrower carbon distribution, more isomers, and can be achieved on Ni with efficiency close to on noble metals. Between the two pathways, hydrocracking is more favored at lower hydrogen pressure (P_{H2}) and with more branched substrates. It accounts for the majority of polypropylene conversion at $P_{H2} \leq$ 30 bar on Ru/TiO_2-A-SG, while is only important at 5 bar with low-density polyethylene and *n*-hexadecane. With low dehydrogenation ability, hydrogenolysis suppresses hydrocracking by reducing free alkene concentration. The hydrocracking activity of Ni/TiO_2-A-SG is higher than a Ni/SSZ-13 we tested, and its evolution with air exposure and calcination suggest that the source of the Brønsted acidity is the carboxylate layers TiO_2 chemisorbs from the air. The investigation of the simultaneous polyolefin hydrocracking and hydrogenolysis on a metal-acid bifunctional catalyst enhances our understanding of the depolymerization chemistry, and guides decisions in process development. The unexpected Brønsted acidity on TiO_2-A-SG revealed in this work also carries significant potentials in other acid-catalyzed reactions.

Acknowledgement

This work was supported by the U.S. Department of Energy (DOE), Office of Science, Office of Basic Energy Sciences (BES), Division of Chemical Sciences, Geosciences and Biosciences, and performed at the Environmental Molecular Sciences Laboratory in (EMSL),

which is a DOE Office of Science User Facility located at Pacific Northwest National Laboratory (PNNL). PNNL is a multiprogram national laboratory operated for DOE by Battelle. O.Y.G. was supported by the DOE, Office of Science, BES, Division of Chemical Sciences, Geosciences and Biosciences (Towards a polyolefin-based refinery: Understanding and controlling the critical reaction steps, FWP 78459). We acknowledge Dr. Johannes A. Lercher, Dr. Lillian V. Hale, and Dr. Sungmin Kim for insightful discussions. We acknowledge Mr. Mark H. Engelhard and Mr. Shari X. Li for XPS and BET measurements.

References

1. Tiseo, I. Annual production of plastics worldwide from 1950 to 2020. (accessed Aug 2022).
2. Barnes, D. K. A.; Galgani, F.; Thompson, R. C.; Barlaz, M., Accumulation and fragmentation of plastic debris in global environments. *Philos. Trans. R. Soc. Lond., B, Biol. Sci.* **2009,** *364* (1526), 1985-1998.
3. Geyer, R.; Jambeck, J. R.; Law, K. L., Production, use, and fate of all plastics ever made. *Sci. Adv.* **2017,** *3* (7), e1700782.
4. Ghaddar, A.; Bousso, R. Rising use of plastics to drive oil demand to 2050: IEA. (accessed Aug 2022).
5. Kaminsky, W.; Schlesselmann, B.; Simon, C., Olefins from polyolefins and mixed plastics by pyrolysis. *J. Anal. Appl. Pyrolysis* **1995,** *32*, 19-27.
6. Bagri, R.; Williams, P. T., Catalytic pyrolysis of polyethylene. *J. Anal. Appl. Pyrolysis* **2002,** *63* (1), 29-41.
7. Kaminsky, W.; Zorriqueta, I.-J. N., Catalytical and thermal pyrolysis of polyolefins. *J. Anal. Appl. Pyrolysis* **2007,** *79* (1), 368-374.
8. Ellis, L. D.; Orski, S. V.; Kenlaw, G. A.; Norman, A. G.; Beers, K. L.; Román-Leshkov, Y.; Beckham, G. T., Tandem Heterogeneous Catalysis for Polyethylene Depolymerization via an Olefin-Intermediate Process. *ACS Sustain. Chem. Eng.* **2021,** *9* (2), 623-628.
9. Ellis, L. D.; Rorrer, N. A.; Sullivan, K. P.; Otto, M.; McGeehan, J. E.; Román-Leshkov, Y.; Wierckx, N.; Beckham, G. T., Chemical and biological catalysis for plastics recycling and upcycling. *Nat. Catal.* **2021,** *4* (7), 539-556.
10. Weitkamp, J., Catalytic Hydrocracking—Mechanisms and Versatility of the Process. *ChemCatChem* **2012,** *4* (3), 292-306.
11. Duan, J.; Chen, W.; Wang, C.; Wang, L.; Liu, Z.; Yi, X.; Fang, W.; Wang, H.; Wei, H.; Xu, S.; Yang, Y.; Yang, Q.; Bao, Z.; Zhang, Z.; Ren, Q.; Zhou, H.; Qin, X.; Zheng, A.; Xiao, F.-S., Coking-Resistant Polyethylene Upcycling Modulated by Zeolite Micropore Diffusion. *J. Am. Chem. Soc.* **2022,** *144* (31), 14269-14277.
12. Rorrer, J. E.; Beckham, G. T.; Román-Leshkov, Y., Conversion of Polyolefin Waste to Liquid Alkanes with Ru-Based Catalysts under Mild Conditions. *JACS Au* **2021,** *1* (1), 8-12.
13. Chen, L.; Zhu, Y.; Meyer, L. C.; Hale, L. V.; Le, T. T.; Karkamkar, A.; Lercher, J. A.; Gutiérrez, O. Y.; Szanyi, J., Effect of reaction conditions on the hydrogenolysis of polypropylene and polyethylene into gas and liquid alkanes. *React. Chem. Eng.* **2022,** *7* (4), 844-854.
14. Xie, T.; Wittreich, G. R.; Vlachos, D. G., Multiscale modeling of hydrogenolysis of ethane and propane on Ru(0001): Implications for plastics recycling. *Appl. Catal., B* **2022,** *316*, 121597.
15. Rorrer, J. E.; Troyano-Valls, C.; Beckham, G. T.; Román-Leshkov, Y., Hydrogenolysis of Polypropylene and Mixed Polyolefin Plastic Waste over Ru/C to Produce Liquid Alkanes. *ACS Sustain. Chem. Eng.* **2021,** *9* (35), 11661-11666.
16. Jia, C.; Xie, S.; Zhang, W.; Intan, N. N.; Sampath, J.; Pfaendtner, J.; Lin, H., Deconstruction of high-density polyethylene into liquid hydrocarbon fuels and lubricants by hydrogenolysis over Ru catalyst. *Chem Catalysis* **2021,** *1* (2), 437-455.

17. Wang, C.; Xie, T.; Kots, P. A.; Vance, B. C.; Yu, K.; Kumar, P.; Fu, J.; Liu, S.; Tsilomelekis, G.; Stach, E. A.; Zheng, W.; Vlachos, D. G., Polyethylene Hydrogenolysis at Mild Conditions over Ruthenium on Tungstated Zirconia. *JACS Au* **2021,** *1* (9), 1422-1434.
18. Celik, G.; Kennedy, R. M.; Hackler, R. A.; Ferrandon, M.; Tennakoon, A.; Patnaik, S.; LaPointe, A. M.; Ammal, S. C.; Heyden, A.; Perras, F. A.; Pruski, M.; Scott, S. L.; Poeppelmeier, K. R.; Sadow, A. D.; Delferro, M., Upcycling Single-Use Polyethylene into High-Quality Liquid Products. *ACS Cent. Sci.* **2019,** *5* (11), 1795-1803.
19. Tennakoon, A.; Wu, X.; Paterson, A. L.; Patnaik, S.; Pei, Y.; LaPointe, A. M.; Ammal, S. C.; Hackler, R. A.; Heyden, A.; Slowing, I. I.; Coates, G. W.; Delferro, M.; Peters, B.; Huang, W.; Sadow, A. D.; Perras, F. A., Catalytic upcycling of high-density polyethylene via a processive mechanism. *Nat. Catal.* **2020,** *3* (11), 893-901.
20. Zhang, F.; Zeng, M.; Yappert, R. D.; Sun, J.; Lee, Y.-H.; LaPointe, A. M.; Peters, B.; Abu-Omar, M. M.; Scott, S. L., Polyethylene upcycling to long-chain alkylaromatics by tandem hydrogenolysis/aromatization. *Science* **2020,** *370* (6515), 437-441.
21. Ertem, S. P.; Onuoha, C. E.; Wang, H.; Hillmyer, M. A.; Reineke, T. M.; Lodge, T. P.; Bates, F. S., Hydrogenolysis of Linear Low-Density Polyethylene during Heterogeneous Catalytic Hydrogen–Deuterium Exchange. *Macromolecules* **2020,** *53* (14), 6043-6055.
22. Nakaji, Y.; Tamura, M.; Miyaoka, S.; Kumagai, S.; Tanji, M.; Nakagawa, Y.; Yoshioka, T.; Tomishige, K., Low-temperature catalytic upgrading of waste polyolefinic plastics into liquid fuels and waxes. *Appl. Catal., B* **2021,** *285*, 119805.
23. Kots, P. A.; Liu, S.; Vance, B. C.; Wang, C.; Sheehan, J. D.; Vlachos, D. G., Polypropylene Plastic Waste Conversion to Lubricants over Ru/TiO2 Catalysts. *ACS Catal.* **2021,** *11* (13), 8104-8115.
24. Wu, X.; Tennakoon, A.; Yappert, R.; Esveld, M.; Ferrandon, M. S.; Hackler, R. A.; LaPointe, A. M.; Heyden, A.; Delferro, M.; Peters, B.; Sadow, A. D.; Huang, W., Size-Controlled Nanoparticles Embedded in a Mesoporous Architecture Leading to Efficient and Selective Hydrogenolysis of Polyolefins. *J. Am. Chem. Soc.* **2022,** *144* (12), 5323-5334.
25. Hackler, R. A.; Lamb, J. V.; Peczak, I. L.; Kennedy, R. M.; Kanbur, U.; LaPointe, A. M.; Poeppelmeier, K. R.; Sadow, A. D.; Delferro, M., Effect of Macro- and Microstructures on Catalytic Hydrogenolysis of Polyolefins. *Macromolecules* **2022,** *55* (15), 6801-6810.
26. Chen, L.; Meyer, L. C.; Kovarik, L.; Meira, D.; Pereira-Hernandez, X. I.; Shi, H.; Khivantsev, K.; Gutiérrez, O. Y.; Szanyi, J., Disordered, Sub-Nanometer Ru Structures on CeO2 are Highly Efficient and Selective Catalysts in Polymer Upcycling by Hydrogenolysis. *ACS Catal.* **2022,** *12* (8), 4618-4627.
27. Vance, B. C.; Kots, P. A.; Wang, C.; Hinton, Z. R.; Quinn, C. M.; Epps, T. H.; Korley, L. T. J.; Vlachos, D. G., Single pot catalyst strategy to branched products via adhesive isomerization and hydrocracking of polyethylene over platinum tungstated zirconia. *Appl. Catal., B* **2021,** *299*, 120483.
28. Jaydev, S. D.; Martín, A. J.; Pérez-Ramírez, J., Direct Conversion of Polypropylene into Liquid Hydrocarbons on Carbon-Supported Platinum Catalysts. *ChemSusChem* **2021,** *14* (23), 5179-5185.
29. Liu, S.; Kots, P. A.; Vance, B. C.; Danielson, A.; Vlachos, D. G., Plastic waste to fuels by hydrocracking at mild conditions. *Sci. Adv.* **2021,** *7* (17), eabf8283.
30. Jumah, A. b.; Tedstone, A. A.; Garforth, A. A., Hydrocracking of virgin and post-consumer polymers. *Microporous Mesoporous Mater.* **2021,** *315*, 110912.

31. Bin Jumah, A.; Anbumuthu, V.; Tedstone, A. A.; Garforth, A. A., Catalyzing the Hydrocracking of Low Density Polyethylene. *Ind. Eng. Chem. Res.* **2019,** *58* (45), 20601-20609.
32. Pyra, K.; Tarach, K. A.; Śrębowata, A.; Melián-Cabrera, I.; Góra-Marek, K., Pd-modified beta zeolite for modulated hydro-cracking of low-density polyethylene into a paraffinic-rich hydrocarbon fuel. *Appl. Catal., B* **2020,** *277*, 119070.
33. Hesse, N. D.; White, R. L., Polyethylene catalytic hydrocracking by PtHZSM-5, PtHY, and PtHMCM-41. *J. Appl. Polym. Sci.* **2004,** *92* (2), 1293-1301.
34. Munir, D.; Irfan, M. F.; Usman, M. R., Hydrocracking of virgin and waste plastics: A detailed review. *Renewable and Sustainable Energy Reviews* **2018,** *90*, 490-515.
35. Ding, W.; Liang, J.; Anderson, L. L., Hydrocracking and Hydroisomerization of High-Density Polyethylene and Waste Plastic over Zeolite and Silica−Alumina-Supported Ni and Ni−Mo Sulfides. *Energy Fuels* **1997,** *11* (6), 1219-1224.
36. Leyva-Porras, C.; Toxqui-Teran, A.; Vega-Becerra, O.; Miki-Yoshida, M.; Rojas-Villalobos, M.; García-Guaderrama, M.; Aguilar-Martínez, J. A., Low-temperature synthesis and characterization of anatase TiO2 nanoparticles by an acid assisted sol–gel method. *J. Alloys Compd.* **2015,** *647*, 627-636.
37. Maesen, T. L. M.; Calero, S.; Schenk, M.; Smit, B., Alkane hydrocracking: shape selectivity or kinetics? *J. Catal.* **2004,** *221* (1), 241-251.
38. Martens, J. A.; Jacobs, P. A.; Weitkamp, J., Attempts to rationalize the distribution of hydrocracked products. I qualitative description of the primary hydrocracking modes of long chain paraffins in open zeolites. *Appl. Catal.* **1986,** *20* (1), 239-281.
39. Alvarez, F.; Ribeiro, F. R.; Perot, G.; Thomazeau, C.; Guisnet, M., Hydroisomerization and Hydrocracking of Alkanes: 7. Influence of the Balance between Acid and Hydrogenating Functions on the Transformation ofn-Decane on PtHY Catalysts. *J. Catal.* **1996,** *162* (2), 179-189.
40. Steijns, M.; Froment, G. F., Hydroisomerization and hydrocracking. 3. Kinetic analysis of rate data for n-decane and n-dodecane. *Ind. Eng. Chem. Prod. Rd.* **1981,** *20* (4), 660-668.
41. Zhou, H.; Chen, L.; Guo, Y.; Liu, X.; Wu, X.-P.; Gong, X.-Q.; Wang, Y., Hydrogenolysis Cleavage of the Csp2–Csp3 Bond over a Metal-Free NbOPO4 Catalyst. *ACS Catal.* **2022,** *12* (9), 4806-4812.
42. Jing, Y.; Wang, Y.; Furukawa, S.; Xia, J.; Sun, C.; Hülsey, M. J.; Wang, H.; Guo, Y.; Liu, X.; Yan, N., Towards the Circular Economy: Converting Aromatic Plastic Waste Back to Arenes over a Ru/Nb2O5 Catalyst. *Angew. Chem. Int. Ed.* **2021,** *60* (10), 5527-5535.
43. Dong, L.; Lin, L.; Han, X.; Si, X.; Liu, X.; Guo, Y.; Lu, F.; Rudić, S.; Parker, S. F.; Yang, S.; Wang, Y., Breaking the Limit of Lignin Monomer Production via Cleavage of Interunit Carbon–Carbon Linkages. *Chem* **2019,** *5* (6), 1521-1536.
44. Cui, Y.; Wang, Y.; Mei, D.; Walter, E. D.; Washton, N. M.; Holladay, J. D.; Wang, Y.; Szanyi, J.; Peden, C. H. F.; Gao, F., Revisiting effects of alkali metal and alkaline earth co-cation additives to Cu/SSZ-13 selective catalytic reduction catalysts. *J. Catal.* **2019,** *378*, 363-375.
45. Chen, L.; Kovarik, L.; Szanyi, J., Temperature-Dependent Communication between Pt/Al2O3 Catalysts and Anatase TiO2 Dilutant: the Effects of Metal Migration and Carbon Transfer on the Reverse Water–Gas Shift Reaction. *ACS Catal.* **2021,** *11* (19), 12058-12067.
46. Yates, J. T., Photochemistry on TiO2: Mechanisms behind the surface chemistry. *Surf. Sci.* **2009,** *603* (10), 1605-1612.

47. Balajka, J.; Hines, M. A.; DeBenedetti, W. J. I.; Komora, M.; Pavelec, J.; Schmid, M.; Diebold, U., High-affinity adsorption leads to molecularly ordered interfaces on TiO2 in air and solution. *Science* **2018,** *361* (6404), 786-789.
48. Flaherty, D. W.; Hibbitts, D. D.; Iglesia, E., Metal-Catalyzed C–C Bond Cleavage in Alkanes: Effects of Methyl Substitution on Transition-State Structures and Stability. *J. Am. Chem. Soc.* **2014,** *136* (27), 9664-9676.
49. Flaherty, D. W.; Iglesia, E., Transition-State Enthalpy and Entropy Effects on Reactivity and Selectivity in Hydrogenolysis of n-Alkanes. *J. Am. Chem. Soc.* **2013,** *135* (49), 18586-18599.
50. Coq, B.; Figueras, F., Structure–activity relationships in catalysis by metals: some aspects of particle size, bimetallic and supports effects. *Coord. Chem. Rev.* **1998,** *178-180*, 1753-1783.
51. Coq, B.; Figueras, F., Influence of the hydrocarbon structure on the hydrogenolysis of alkanes over rhodium/alumina catalysts. *J. Mol. Catal.* **1987,** *40* (1), 93-112.
52. Zhou, Z.; Pesek, S.; Klosin, J.; Rosen, M. S.; Mukhopadhyay, S.; Cong, R.; Baugh, D.; Winniford, B.; Brown, H.; Xu, K., Long Chain Branching Detection and Quantification in LDPE with Special Solvents, Polarization Transfer Techniques, and Inverse Gated 13C NMR Spectroscopy. *Macromolecules* **2018,** *51* (21), 8443-8454.
53. Nakagawa, Y.; Oya, S.-i.; Kanno, D.; Nakaji, Y.; Tamura, M.; Tomishige, K., Regioselectivity and Reaction Mechanism of Ru-Catalyzed Hydrogenolysis of Squalane and Model Alkanes. *ChemSusChem* **2017,** *10* (1), 189-198.
54. Coq, B.; Bittar, A.; Dutartre, R.; Figueras, F., Influence of the precursor and the support on the catalytic properties of ruthenium for alkane hydrogenolysis. *Appl. Catal.* **1990,** *60* (1), 33-46.
55. Wang, R.; Hashimoto, K.; Fujishima, A.; Chikuni, M.; Kojima, E.; Kitamura, A.; Shimohigoshi, M.; Watanabe, T., Light-induced amphiphilic surfaces. *Nature* **1997,** *388* (6641), 431-432.
56. Khare, P.; Kumar, N.; Kumari, K. M.; Srivastava, S. S., Atmospheric formic and acetic acids: An overview. *Rev. Geophys.* **1999,** *37* (2), 227-248.